Sensitivity of Aromatic Carbon in Sugarcane Mill Mud to Photolysis within the Visible Range

Minori Uchimiya [a,*] and Kaitlyn Taylor [b]

*Corresponding author: sophie.uchimiya@usda.gov

DOI: 10.15376/biores.21.2.5057-5070

GRAPHICAL ABSTRACT

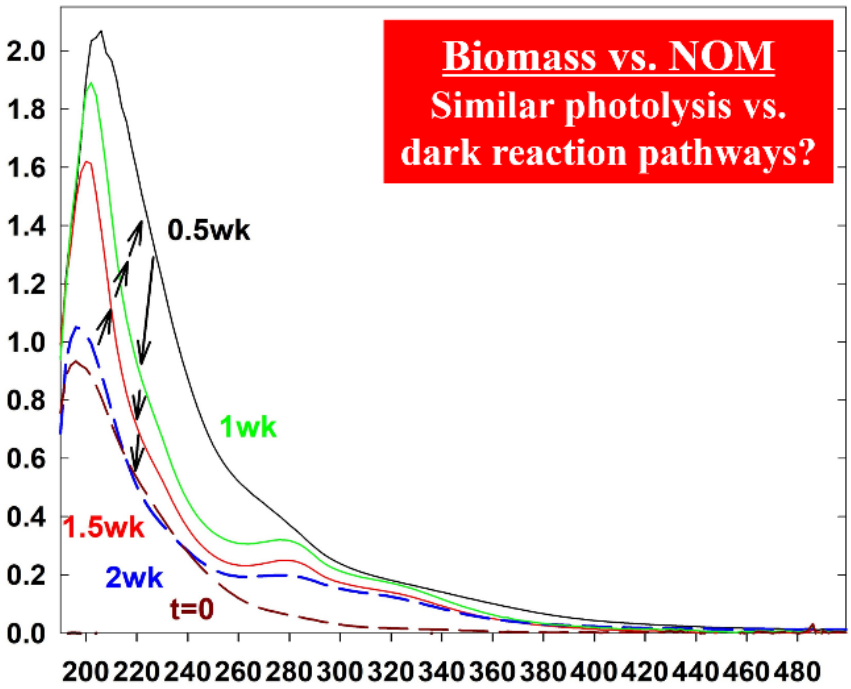

Sensitivity of Aromatic Carbon in Sugarcane Mill Mud to Photolysis within the Visible Range

Minori Uchimiya [a,*] and Kaitlyn Taylor [b]

Direct and indirect photolysis are the primary fate pathways of natural organic matter (NOM) impacting the global carbon cycle in surface soils. For NOM, opposite trends in structural changes are often observed between photolytic and dark aerobic transformations. Industrial organic byproducts are generated under more controlled conditions than NOM, and their photochemical fate is largely unknown. This study employed optical methods (fluorescence, UV/visible) to trace the changes in conjugated structures of sugar processing byproduct (mill mud) for 2 wk. After an initial (≈1 wk) lag period, photolysis became dominant over dark reactions. Photolysis increased the aromaticity (higher emission wavelength peaks) and estimated amount (higher fluorescence intensity) of chromophores, and the effects were greater for pristine than aged mill mud. However, field aging of mill mud transformed reactive chromophores into stable aromatic structures with characteristic ≈400 nm emission that were resistant to photolysis or dark reaction. Factory mill mud showed similar fate pathways as NOM. Anaerobic incubation in dark formed absorbance peaks at 280 and 320 nm typically observed in NOM. Slope ratios for those peaks were decreased by photolysis, indicating the formation of aromatic structures. In summary, visible range irradiation is sensitive to conjugated double bonds, and could be used to add values to industrial byproducts, and to evaluate their fate as a soil amendment.

DOI: 10.15376/biores.21.2.5057-5070

Keywords: Fertilizer; Soil amendment; Environmental fate; Optical methods; Soil organic carbon

Contact information: a: United States Department of Agriculture, Agricultural Research Service, Southern Regional Research Center, 1100 Allen Toussaint Boulevard, New Orleans, LA 70124 USA; b: Oak Ridge Institute for Science and Education Research Program at USDA, Oak Ridge, TN 37831 USA;
** Corresponding author: sophie.uchimiya@usda.gov*

INTRODUCTION

A large number of studies have been conducted on photobleaching of naturally occurring dissolved organic carbon (DOC) chromophores in aquatic and terrestrial environments (Helms *et al*. 2008). Photolysis is a major abiotic DOC transformation pathway in surface soil, while redox reactions become important in subsurface under anoxic conditions. Limited information is available to understand the photochemical fate of land-applied industrial biomass byproducts. Mill mud is generated as pressed slurry from heated clarifiers at sugarcane factories. Microbial composition of mill mud is controlled by the high temperature factory operation to produce raw sugar from extracted sugarcane juice The authors previously reported on a series of studies characterizing sugarcane mill mud byproducts from U.S. raw sugar factories (Uchimiya *et al*. 2022). Sugarcane mill mud from Louisiana and Florida had high (on dry weight basis) phosphorus (≈2% as P_2O_5) and organic matter (>50%), regardless of the factory origin (Uchimiya *et*

al. 2022). Fresh mill mud collected indoors at the operating factories had probiotic effects on soybean growth (Uchimiya *et al*. 2023), and underwent maturity processes similar to composts correlating with exposed operational temperatures (Uchimiya *et al*. 2024). Bio-fertilizer and bio-stimulant could be developed from sugarcane mill mud/filter cake to provide (1) carbon source for soil microbiome to promote soil health and (2) controlled-release of PKN and other essential plant nutrients to reduce the cost to purchase imported inorganic fertilizers. In Louisiana, waste management for mill mud has become expensive at mills, as on-site waste piling space is becoming exhausted.

The objective of the present study was to understand the environmental fate of fresh mill mud, focused on photochemistry of chromophores. Mill mud is exposed to sunlight during months- to years-long storage as dry piles or in waste ponds as slurries (Uchimiya *et al*. 2022). When applied to surface soils, mill mad can engage in direct and indirect photolysis (Pignatello *et al*. 2024). Direct photolysis chemically transforms the light-absorbing reactants, *i.e.*, chromophores. Indirect photolysis is a chain reaction involving free radicals and other redox-active intermediates (Sharpless *et al*. 2014; Buckley *et al*. 2024). The relative importance of photolysis and dark transformation is entirely unknown for mill mud applied to sugarcane fields alone or after mixing/composting with mill ash and bagasse in the U.S. (Florida, and Louisiana to a lesser extent) (Gilbert *et al*. 2008).

Regardless of the type of biomass or its environmental origin, DOC is a complex mixture of chromophores with different molar absorptivities (ε) (Yan *et al*. 2025). Although Beer's law is not followed and contribution of individual molecules in a mixture is likely not additive, UV/Visible absorbance is the standard method to follow the photolysis kinetics of DOC. Conjugated double bonds increase the peak wavelength and molar absorptivity of a molecule. Each additional double bond in a conjugated π-electron system is estimated to shift the absorption maximum by 30 nm and double the molar absorptivity (Yan *et al*. 2025). Similarly, conjugated bonds red-shift the fluorescence excitation and emission (EEM) wavelengths and increase the quantum yield of a molecule (Lichtman and Conchello 2005). As a result, UV/Visible and fluorescence methods are widely used to trace the changes in DOC structures by photolysis and to estimate the degree of aromaticity (Buckley *et al*. 2024). Absorbance (UV/Visible) spectra can be used to detect the reactive chromophores. Emission (fluorescence) spectra detect the structural changes at photosensitive excitation wavelengths. Of various UV/Visible parameters proposed to trace photolysis kinetics, spectral slope measures the change in absorbance within a specific wavelength range (Yan *et al*. 2025). Spectral slope is inversely correlated with the average molecular weight of DOC and molar absorptivity for frequently observed major (≈275 nm) and minor (≈380 nm) DOC peaks (Yan *et al*. 2025). Opposite changes in the spectral slope were observed in photolysis and dark (aerobic microbial) decomposition of river and ocean DOC in controlled laboratory experiments (Helms *et al*. 2008). The slope ratio for shorter (275 to 295 nm) to longer (350 to 400 nm) wavelengths increased with time during photolysis, and decreased during aerobic incubation (Helms *et al*. 2008). The results were attributed to increased degree of conjugation in DOC products of dark reactions (Helms *et al*. 2008).

The present study tested the hypothesis that photolysis and dark reaction of industrial byproduct (sugarcane mill mud) follow the structural trends observed for natural organic matter (NOM) in soils and sediments. Sugarcane mill mud is produced under more controlled environment (factory) than NOM, and high temperature operation controls its initial microbiome (Uchimiya *et al*. 2022) engaging in aerobic reaction in dark. In this study, time courses of photolysis and dark reaction were monitored by UV/Visible spectral

trends reflecting the changes in reactive chromophores. Fluorescence can provide snapshots of aromatic structure formation and decomposition as emission peaks at a given photosensitive (excitation) wavelength. In the literature, mass spectroscopy-based non-targeted analysis has been used to detect photolysis products (Zherebker *et al*. 2020). Optical methods (simplest) and non-targeted analysis (generating tens of thousands of chemical features) represent the opposite ends of complexity in monitoring photochemistry. Because DOC is inherently complex, identification of reactive functionality and interpretation heavily rely on correlation analysis for either approach. Data reduction is essential for interpreting mass spectroscopy data in non-targeted analysis. Optical method relies on wavelength-dependent interpretation of bulk functionalities.

EXPERIMENTAL

Mill mud collection, handling, and characterization followed previously described methods (Uchimiya *et al*. 2022). During the 2023 sugarcane harvest season in Louisiana, fresh mill mud samples were collected from 2 separate operating factories in Louisiana, directly from the heated conveyor belt press filter: Mud-LA2-2023 and Mud-LA3-2023 (analogous to Mud-LA2 and Mud-LA3 collected in 2019 (Uchimiya *et al*. 2022)). Third mill mud sample was obtained from a pile at a commercial sugarcane field growing the variety CP 96-1252 in Florida. The mill mud pile was 2 years old, and it was intended for application to the surface soil at the ratio of mill mud:mill ash:bagasse = 3:3:6 (in inches). The factory source of this field-aged mill mud sample (Mud-FL1-2023) is analogous to Mud-FL1 collected in 2019. As-received Mud-LA2-2023 (64% moisture), Mud-LA3-2023 (75% moisture), and Mud-FL1-2023 (53% moisture) were stored at -15 °C until analyses. All laboratory procedures used distilled, deionized water (DDW) with a resistivity of 18 MΩ cm (APS Water Services, Van Nuys, CA). All chemical reagents were obtained from Sigma-Aldrich (Milwaukee, WI) with the highest purity available.

Photolysis Experiments

Using Mud-LA3-2023 (pH 5.1) as a representative factory mill mud (without environmental exposure), three separate kinetic procedures were independently tested: photolysis ("1sun"); dark aerobic incubation as a control ("dark"); and photolysis after the dark reaction ("dark, 1sun"). LED (400 to 1100 nm) solar simulator (LSH-7320, Newport, Bozeman, MT) was used as the irradiation source in experiments involving "1sun". Mill mud (100 g/L in DDW) was magnetically stirred (600 rpm) under continuous 1sun (100 mW/cm^2) irradiation for 14 d in a glass beaker with glass lid and daily replacement of evaporated water. Experiments were conducted at room temperature and pH was set by the high mill mud loading without added buffer. A known volume of homogeneous slurry was sampled (before (t=0), after (14 d), and at selected timepoints in between) using a disposable syringe, filtered (0.45 μm PTFE, Fisher, Hampton, NH), and immediately analyzed spectrophotometrically after 5 to 10-fold DDW dilution. As a control without photolysis, "dark" experiments were employed using analogous procedures without irradiation, where the reactor was triply wrapped with aluminum foil. To test the photolysis of end-product from "dark" experiment, "dark, 1sun" used the remaining slurry from completed (after 2 wk) "dark" experiment as the starting material at t=0 to initiate the "1sun" procedure described above.

Fluorescence Spectral Tracing of Photolysis Over Time

As detailed previously (Uchimiya and Knoll 2019), scattering, quenching, and inner-filtering become significant enough to violate the Beer-Lambert law for concentrated, turbid, and colloidal aqueous samples. In the present study, successive dilution showed no shifts in fluorescence peaks. In addition to the sample dilution, reflective emission measurement was used to minimize the influence of non-fluorescence disturbance. Reflective EEM uses light beam irradiation at 30°, and reflection at -60°, along the center line of the quartz cell window; this design prevents the reflected light beam from reaching the light detector.

Fluorescence spectra were collected using F-7000 spectrofluorometer (Hitachi, San Jose, CA) at 220 to 598 nm excitation and 280 to 730 nm emission wavelengths in 3 nm intervals; 5 nm excitation and emission slits; auto response time; and 2400 nm min^{-1} scan rate (Uchimiya and Knoll 2019).

A blank spectrum was collected daily for DDW and was subtracted from samples to correct for the background and to remove Rayleigh and Raman peaks. Sample spectra were additionally pre-processed using first and second order Rayleigh (20 nm) and Raman (10 nm) filters, for first order Raman shift (3382/cm), and by assigning zero to sub-Rayleigh and supra-second order Rayleigh wavelengths.

Parallel factor (PARAFAC, n=32) analysis was performed with non-negativity constraint using MATLAB version 23.2 (R2023b; Mathworks, Natick, MA) with PLS toolbox version 9.3 (Eigenvector Research, Manson, WA). Three component models were selected based on the core consistency (96) and residual analysis. Absolute and fractional (normalized to the total intensity of a given sample) contributions of PARAFAC fingerprints were used to interpret the relative changes in PARAFAC components as a function of time.

UV/Visible Absorbance Parameters

UV/Visible spectra (HP8452A, Hewlett-Packard, Palo Alto, CA) were obtained using 10 mm path length quartz cell after blank subtraction with DDW. Spectral slope of UV/Visible absorbance was calculated following the literature method (Yan *et al*. 2025). The absorption coefficient ($a(\lambda)$ in $1/m$) was calculated as: $a(\lambda) = 2.303*(\text{Abs}(\lambda)/L)$, where $\text{Abs}(\lambda)$ is dimensionless absorbance at λ nm and L is the cell path length of the cuvette. The spectral slope ($S_{\lambda 1-\lambda 2}$) was calculated as: $S_{\lambda 1-\lambda 2} = -((\ln a(\lambda_1)-\ln a(\lambda_2))/(\lambda_1-\lambda_2))$. Three wavelength ranges were selected to calculate slopes: 275 to 295 nm (S1) and 350 to 400 nm (S2) based on the literature (Helms *et al*. 2008; Yan *et al*. 2025), and 300 to 330 nm (S3) based on the peak observed in the present study for sugarcane mill mud. The peak area typically increases at lower wavelengths, and the slope ratios of major and minor peaks were calculated as: S1/S2 and S1/S3 (Helms *et al*. 2008).

UV/Visible spectral parameters (S1, S2, S3, S1/S2, S1/S3) and fluorescence EEM/PARAFAC contributions (factors 1-3 in absolute and normalized contributions, and total fluorescence intensity of each sample) were statistically analyzed for sample (Mud-LA2-2023, Mud-LA3-2023, and Mud-FL1-2023), sampling time (t=0, 1 wk, 1.5 wk, and 2 wk), and reaction type (dark, 1sun, and dark,1sun) main effects ANOVA using Statistica version 12 (Statsoft, Tulsa, OK) at a significance level of $P<0.05$. If significant difference was indicated by the standardized range distribution, post hoc comparison was conducted using Tukey's honestly significant difference (HSD) test.

RESULTS AND DISCUSSION

Timecourses of Mill Mud Photolysis

Figure 1 shows the timecourses of dark (a), 1sun (b), and dark, 1sun (c) reactions for Mud-LA3-2023. Each panel of Fig. 1 represents separate reactors, and comparisons will be made based on the changes in spectral features (within and between panels) and absorbance (for a given panel). In each panel of Fig. 1, sampling time (t=0 and 0.5, 1, 1.5, 2 wk) is color-coded, and absorbance increase (↑), decrease (↓), or no change (≈) are visually assigned. Dashed vertical lines in Fig. 1 show a peak for S1 near 280 nm and a minor peak for S3 near 320 nm.

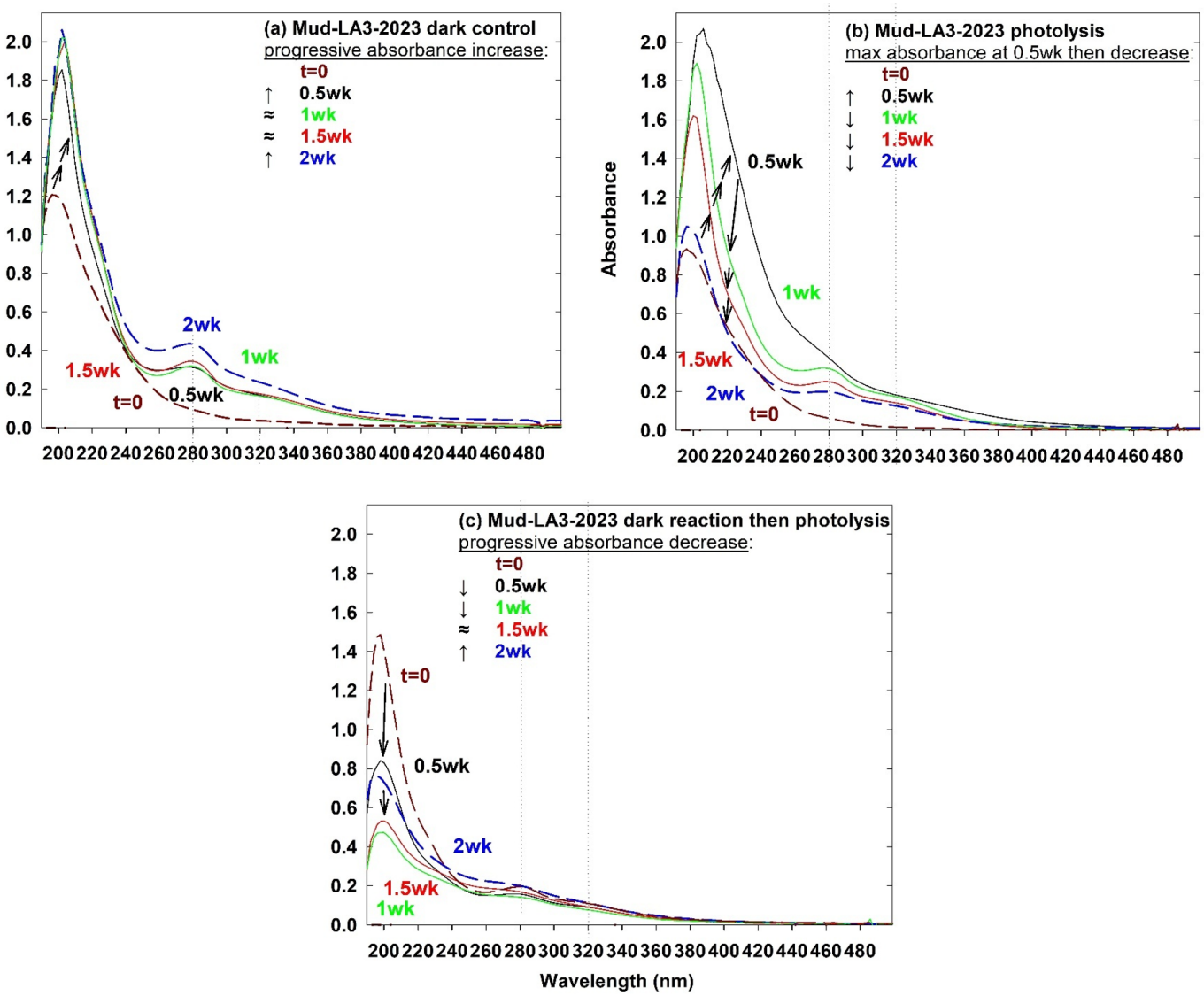

Fig. 1. Timecourses of aerobic incubation in dark (a), photolysis at 100 mW/cm^2 (b), and photolysis after the dark reaction (c) for fresh mill mud collected within the operating factory (Mud-LA3-2023; 100 g/L for 2 wk). Dashed vertical lines show peak maxima for S1 (275-295 nm) and S3 (300-330 nm). In each panel, arrows on spectra follow absorbance changes as a function of time, and are summarized as increase (↑), decrease (↓), or no change (≈) in legend, where sampling time is color-coded with spectrum.

Figure 1a (dark control) indicates progressive absorbance increases as a function of time for both peaks and at lower wavelengths. For 1sun (Fig. 1b), an initial absorbance increase (at 0.5 wk) was followed by progressive decreases over 2 wk period. Comparison of Figs. 1a-1b suggests that after an initial absorbance increase by dark reactions (up to 0.5 wk), photolytic decomposition became dominant to produce lower absorbing chromophores. When 2 wk end-product of dark reaction is photolyzed (Fig. 1c) using the same procedures as Fig. 1b, the absorbance further decreased, although a subsequent increase is observable from 1.5 to 2 wk.

Figure 2 shows reactions analogous to Figs. 1a-1b for Mud-LA2-2023 collected from a different factory. Before the reaction (t=0), DOC of two fresh mill mud samples had similar spectra (brown lines in Figs. 1a and 2a). Lower peak absorbance of Mud-LA2-2023 (≈0.6 near 200 nm in Fig. 2a) suggests lower extractable DOC (Uchimiya *et al*. 2013) than Mud-LA3-2023 (≈1.2 in Fig. 1a). Figure A.1 shows the elemental composition of two factory mill mud samples. The sample with higher DOC at t=0 (Mud-LA3-2023) shows organic characteristics and has higher carbon, organic matter, and C:N than Mud-LA2-2023 dominated by inorganic components (Fe, Cu, Al, Mg, Mn) in Fig. A.1. Time trends are similar for both mill mud samples in each (dark and 1sun) reaction. Absorbance increased with time in the dark control (Fig. 2a), while an initial increase was followed by a decrease in 1sun (Fig. 2b). Collectively, Mud-LA3-2023 had higher organic matter and DOC than Mud-LA2-2023 before the reaction, and both reactants showed similar time trends in both dark and photolysis experiments.

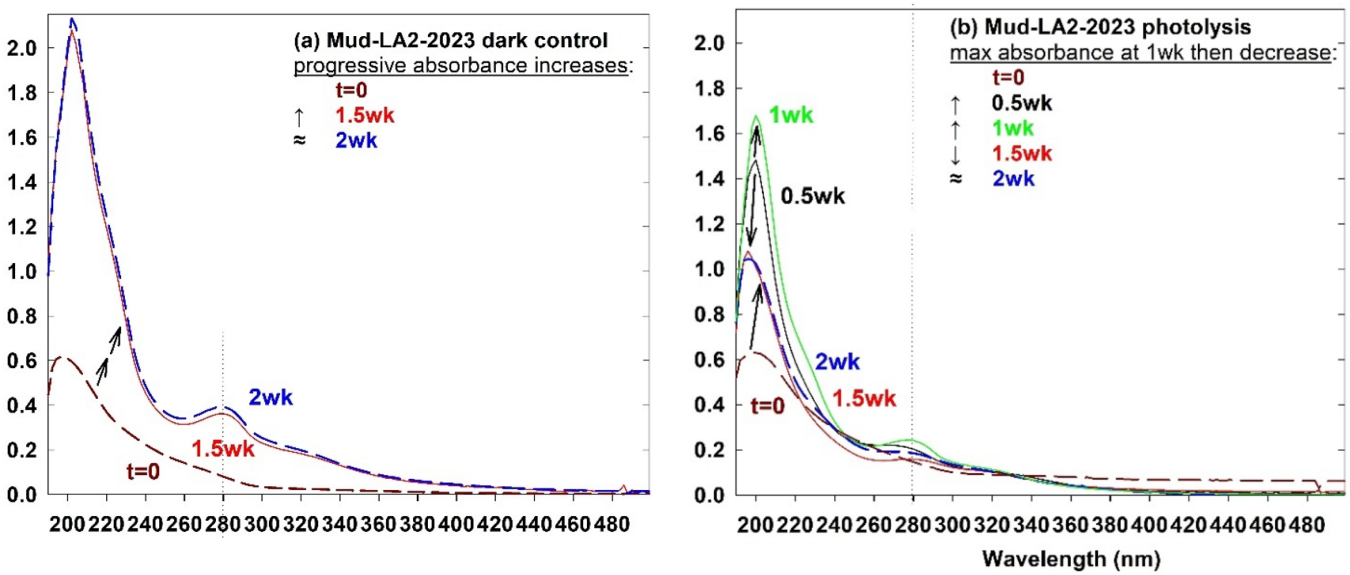

Fig. 2. Timecourses of dark control (a), and photolysis (b) for the second fresh mill mud Mud-LA2-2023, using analogous procedures as in Fig. 1. Dashed vertical line shows S1 peak maximum near 280 nm.

Figures 3 and 4 show fluorescence spectra corresponding to the reactions presented in Figs. 1 and 2. In each panel of Figs. 3 and 4, primary peaks are indicated by arrows as: excitation/emission wavelengths (fluorescence intensity). Figures 3a to 3c show time courses of fluorescence spectra in dark control corresponding to Fig. 1a. Fluorescence peak positions for the dark anaerobic incubation did not change, except for the formation of minor peak at higher wavelength (345Ex/430Em) after 2 wk. Intensity of the primary peak

near 275Ex/340Em slightly increased after 0.5 wk and then slightly decreased. For photolysis in Figs. 3d-3f, the initial (at t=0) primary peak at 275Ex/340Em disappeared after 0.5 wk to form a new peak at lower Em (275/310) and two additional peaks (250/400, 310/400). Subsequently at 2 wk (Fig. 3f), all three new peaks disappeared, and the spectrum returned to the same peak position and intensity (275/350 (1280)) as before photolysis (*t*=0 in Fig. 3d). When the product of dark control (Fig. 3c) was photolyzed in Figs. 3g-3i, fluorescence intensity became negligibly low (≈260 maximum in the spectrum shown in Fig. 3i), and the original peaks at 275Ex/360Em and 275Ex/310Em disappeared after 2wk of photolysis. Collectively, UV/Visible and fluorescence spectra complementarily revealed the following trends. First, aerobic incubation in dark increased the intensity of chromophore(s) absorbing at ≈280 nm, as indicated by increased absorbance of S1 peak as a function of time in Fig. 1a, and by changes in the fluorescence intensity of the primary peak in Figs. 3a-3c. Time trends in UV/Visible spectra suggest that photolysis outweighs the dark reaction at later (≥1 wk) stage to initiate the decomposition of conjugated chromophores (Fig. 1). Fluorescence spectra in Figs. 3d to 3f revealed the formation of new, higher (400 nm) and lower (310 nm) Em peaks during photolysis (Fig. 3e) but not in the dark control (Fig. 3b). End-product (2 wk) of dark reaction was photolyzed more readily (resulting in the lowest maximum intensity in panel i, among all spectra presented in Fig. 3) than fresh mill mud (Figs. 3d to 3f).

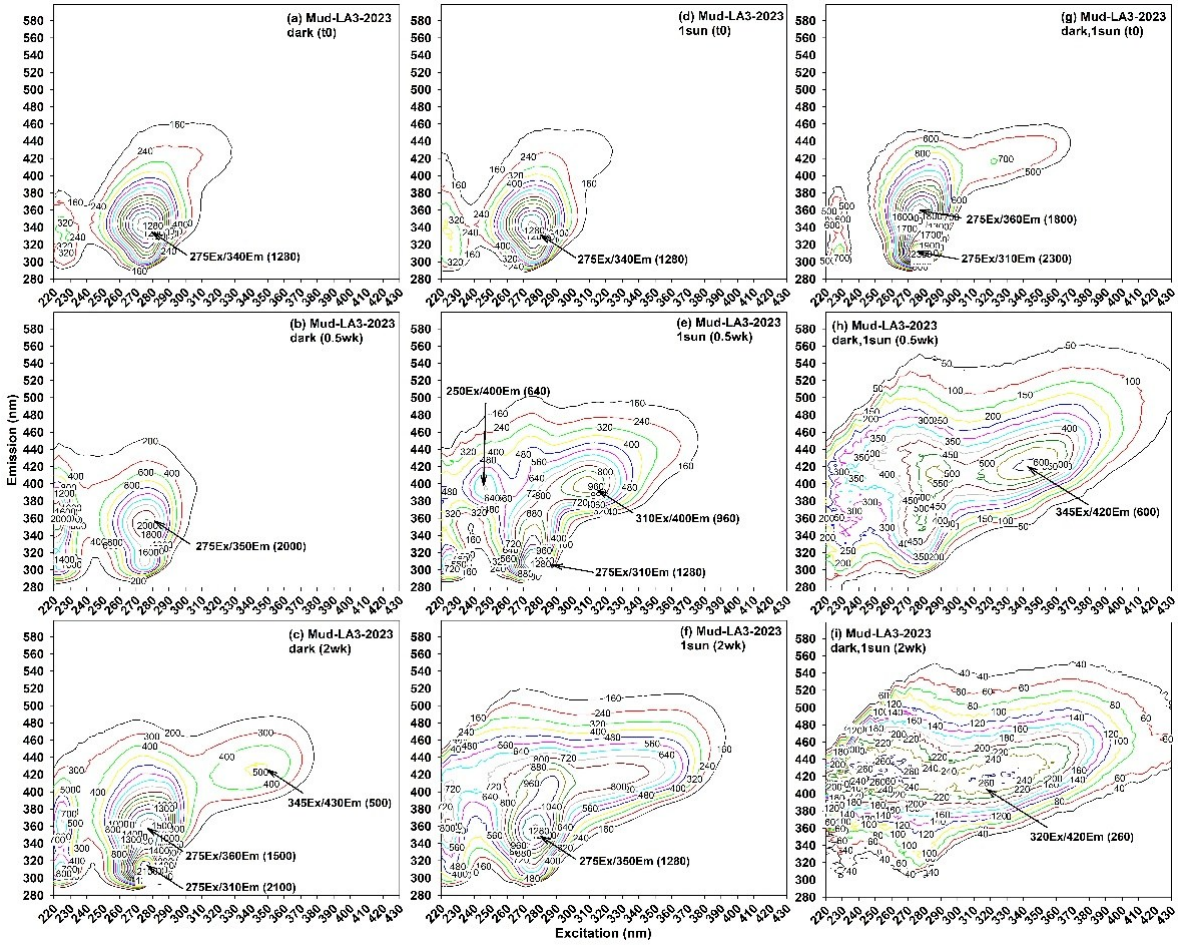

Fig. 3. Fluorescence monitoring of Mud-LA3-2023 reactions in Fig. 1 corresponding to dark (a-c), photolysis (d-f), and photolysis of dark reaction products (g-i)

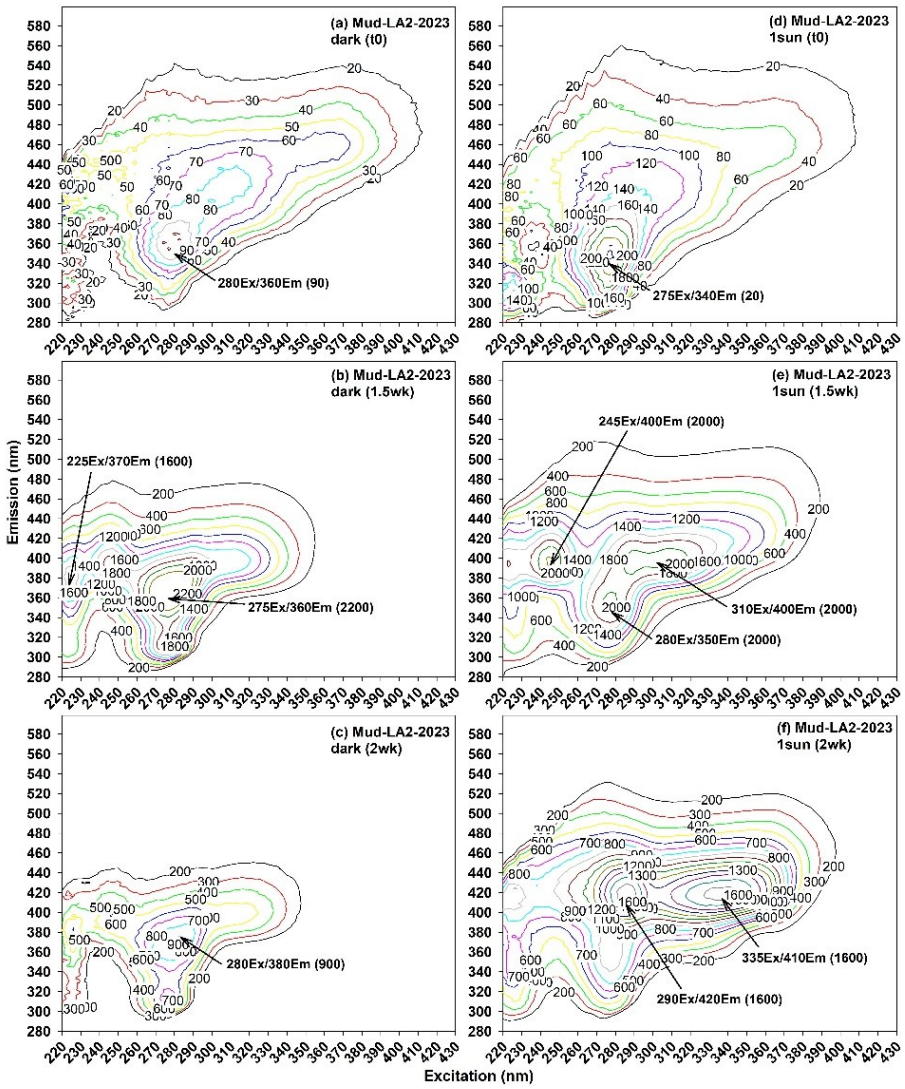

Fig. 4. Fluorescence snapshots of Mud-LA2-2023 reactions corresponding to Fig. 2. Formation of new, higher emission peaks are observable during photolysis (e-f) but not in dark control (b-c).

Similar trends were observed for Mud-LA2-2023 in Fig. 4. Before reactions, fluorescence spectrum of Mud-LA2-2023 (Fig. 4a) had orders of magnitude lower intensity than Mud-LA3-2023 (Fig. 3a) at analogous Ex/Em position, in agreement with the absorbance intensities of corresponding UV/Visible spectra in Figs. 1 and 2. Dark reactions in Figs. 4a-4c increased (at 1.5 wk) and then decreased (after 2 wk) the peak intensities. Peak intensity increased more dramatically for Mud-LA2-2023 (by over an order of magnitude after 1.5 wk dark reaction in Fig. 4b) than Mud-LA3-2023, which was likely due to lower fluorescence of Mud-LA2-2023 before the reaction. Photolysis of Mud-LA2-2023 (Figs. 4d to 4f) led to the formation of several new high intensity peaks at higher Ex/Em in Figs. 4e and 4f. Those results show the formation of higher aromaticity photochemical products. In summary, consistent time trends and structural changes are observed for factory mill mud with higher (Mud-LA3-2023) and lower (Mud-LA2-2023) initial DOC contents. Fluorescence captured the formation of several new and conjugated products because of photolysis, but not in the dark control.

Figure 5 shows analogous plots for aged sample (Mud-FL1-2023) collected from a two-year-old mill mud pile at sugarcane field. In contrast to fresh mill mud in preceding figures (Mud-LA2-2023, Mud-LA3-2023), S1 and S3 peaks were not visible in dark reaction (Fig. 5a) or photolysis (Fig. 5b). However, time trends in UV/Visible absorbance are similar to fresh mill mud for both reactions in Figs. 1-2. Aerobic incubation in the dark increased the peak near 210 nm, while photolysis increased and then decreased the peak. Corresponding EEM spectra in Figs. 5c-5h do not show new peak formation for dark control or photolysis. In photolysis (Figs. 5f-5h), single peak near 270/440 remained at a stable intensity over 2 wk. Those results suggest that field aging of mill mud removed chromophores reactive towards both photolysis and aerobic transformation in dark. Field aging of factory mill mud likely formed a stable (400 to 440 Em) aromatic structure resistant to photolysis or dark biotic/abiotic decomposition.

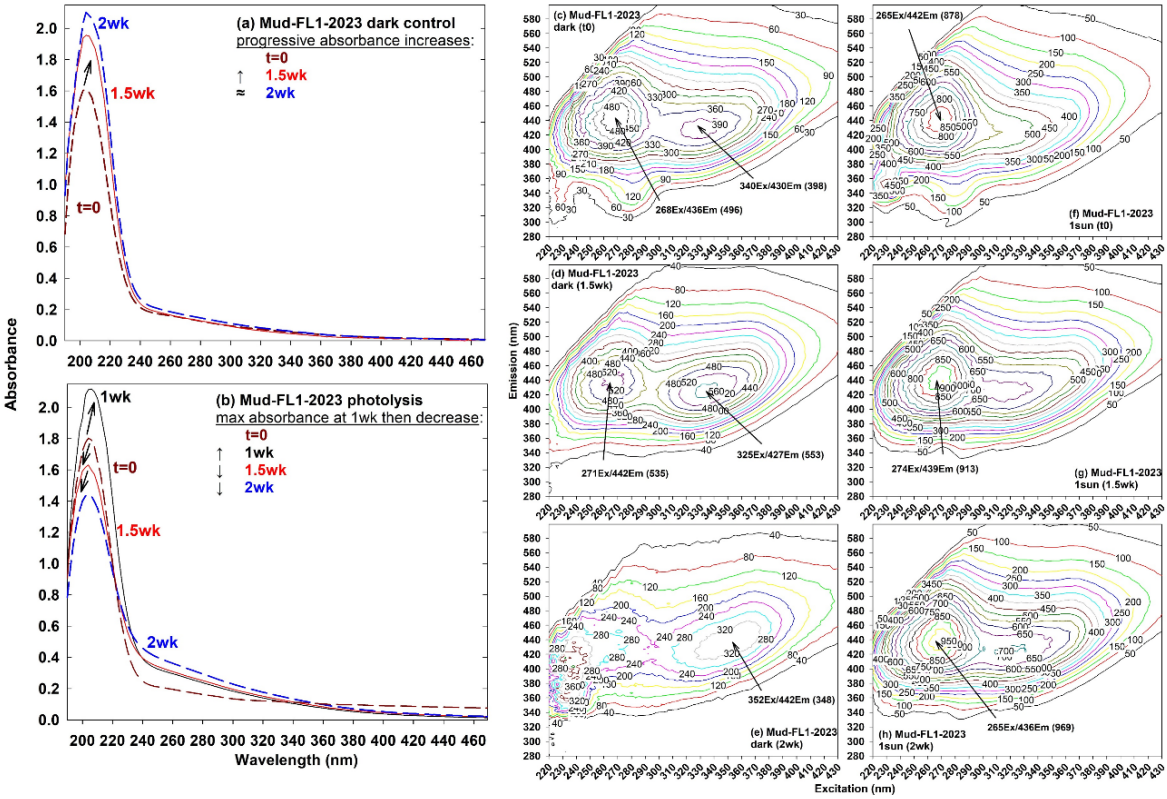

Fig. 5. UV/Visible (a-b) and EEM (c-h) tracings of Mud-FL1-2023 aged for 2 years in sugarcane field. Unlike factory mill mud in Figs. 1-2, S1 and S3 peaks are absent in aged mill mud (a-b), and no new peak is formed by photolysis (g-h).

Statistical Analysis

Figure 6 shows PARAFAC fingerprints with progressively higher excitation and emission wavelengths hereby assigned to: aliphatic (a), mid EEM (b), and aromatic (c) bulk structural fingerprints. Those PARAFAC fingerprints are used to statistically ($P < 0.05$) interpret the changes in aromaticity by main effects ANOVA in Table 1. Each column of Table 1 shows significant p-values (<0.05) and differences by post hoc Tukey tests for mill mud (n=3), reaction (photolysis, dark, and photolysis of dark reaction end product, n=3), and sampling time (t0 and 1-2 wk) main effects.

Table 1. Significant p-Values (<0.05; post-hoc Tukey indicated as >,<) for the Effects of Mill Mud Source, Reaction Type, and Sampling Timepoint (columns) on Fluorescence and UV/visible Spectra of Fresh (Mud-LA2-2023 and Mud-LA3-2023 Collected Inside the Factories) and Aged (Mud-FL1-2023 aged outdoor for 2 years) Sugarcane Mill Mud Extracts (n=30 for all variables)

Variable	Mean	S.D.	Min	Max	Mill Mud	Reaction ; Time
Fluorescence PARAFAC Factors						*Reaction*
1 (Aliphatic)	15158	15152	367	58470	0.022 (Mud-FL1-2023<Mud-LA2-2023,Mud-LA3-2023)	
%1 (Aliphatic)	35	25	1	76	<1e-5 (Mud-FL1-2023<Mud-LA2-2023,Mud-LA3-2023)	<2e-4 (dark>dark,1sun)
%2 (Mid EEM)	29	11	13	55	0.012 (Mud-LA2-2023>Mud-LA3-2023)	
3 (Aromatic)	11590	7982	437	27577	0.019 (Mud-FL1-2023>Mud-LA2-2023,Mud-LA3-2023)	<1e-3 (1sun>dark)
%3 (Aromatic)	36	23	1	71	<1e-5 (Mud-FL1-2023>Mud-LA2-2023,Mud-LA3-2023)	<4e-4 (dark,1sun>dark)
Total Intensity	37671	21557	3990	82127		0.033 (1sun>dark,1sun)
Slope Of ln(Absorbance) in UV/Visible Spectra						*Time*
S1 (275-295nm)	2E-02	7E-03	9E-03	4E-02	0.032 (Mud-LA2-2023>Mud-FL1-2023)	0.045 (t0>2wk)
S1/S2 (350-400nm)	1.0	0.9	0.4	4.7		0.008 (t0>1wk,1.5wk,2wk)
S1/S3 (300-330nm)	1.4	0.8	0.7	4.3		0.022 (t0>2wk)

Each column shows significant p-values (<0.05) and differences by post hoc Tukey tests for mill mud (n=3), reaction (photolysis, dark, and photolysis of dark reaction end product, n=3), and sampling time (*t* =0 and 1-2 wk) main effects.

Table 1 indicates the increase in aromaticity of DOC in mill mud with time, as indicated by the decrease in S1/S2 and S1/S3 ratios after the reactions. Highest and lowest S1 peak in Mud-LA2-2023 and Mud-FL1-2023, respectively, were described in preceding sections and were statistically significant in Table 1.

For PARAFAC factors, the mill mud main effects column in Table 1 indicates an increase in aromaticity from Mud-FL1-2023, Mud-LA3-2023, to Mud-LA2-2023. Photolysis formed more aromatic structures than the dark control. In addition, total fluorescence intensity was higher for photolysis of pristine mill mud than the aged (underwent dark reaction) mill mud.

Relative fraction of aromatic structure at each sampling time point (3% PARAFAC fingerprint) increased when the 2 wk end-product of dark reaction was photolyzed. This is observable in Fig. 3, where "dark, 1sun" reaction led to the formation of highest Ex/Em peak (345/420) of all fluorescence spectra collected in this study. Finally, relative proportion of aliphatic fingerprint (1% in Table 1) decreased by photolysis after the dark experiment, in agreement with raw spectra presented in Fig. 3.

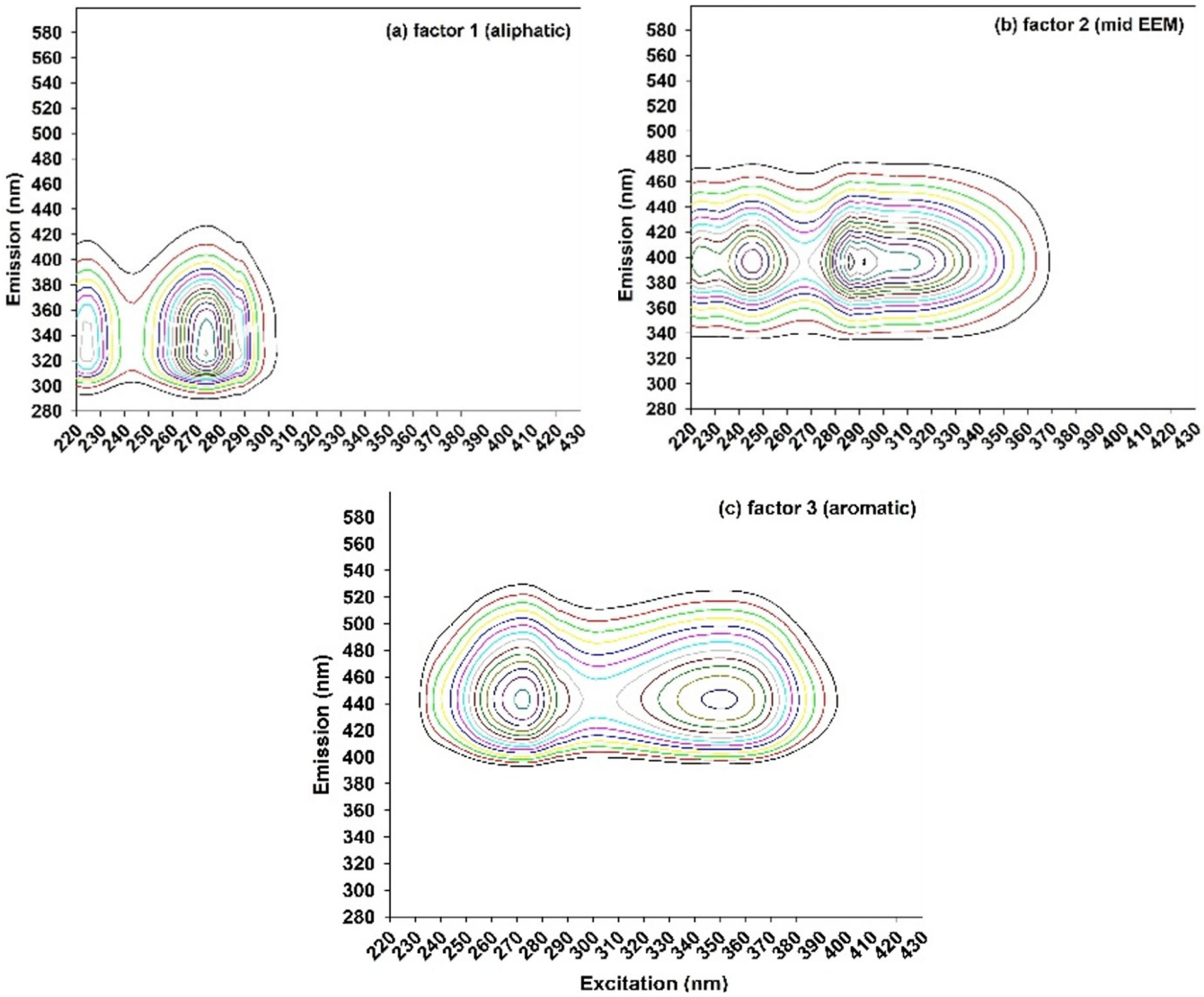

Fig. 6. Three PARAFAC fingerprints obtained from all kinetic experiments presented in this study (96 core consistency). Factors 1 to 3 represent fingerprints with progressively higher degree of conjugation, as indicated by higher excitation and emission wavelengths.

Laser irradiation and xenon arc lamp solar simulator are traditionally used to study the photochemical transformation of soil organic carbon. Limited reports on visible range irradiation offer insights into the observations from the present study. Light emitting diode (LED) simulated sunlight was used to understand the production of photochemically produced reactive intermediates within visible wavelengths (Wu *et al*. 2021). Aromatic structures are more sensitive to photolysis within the visible range than lower wavelengths (Del Vecchio and Blough 2004). Absorption loss maximum of NOM shifted from 250 to 400 nm by laser irradiation at lower wavelengths (260 to 360 nm) to broader ranges (250 to 550 nm) by >500 nm irradiation (Del Vecchio and Blough 2004). Visible range irradiation (≥460 nm) forms condensed structures with decreased oxygen functional groups (Zherebker *et al*. 2020). Carboxylate-substituted unsaturated and aromatic carbon is thought to be the reactive electron acceptor (Zherebker *et al*. 2020). The observations in the literature and the present study suggest a potential application of visible range irradiation for valorization of biomass. Aromatic, condensed structure is the key product

specification for bio-stimulants. Visible range LED irradiation could offer a new, energy-efficient and safer (*vs.* high intensity xenon/mercury arc lamp) method to stabilize biomass for agricultural applications. Potential risk of photochemically activated biomass for soil application include persistent free radical contents and unintended release of heavy metals by chelation. Those and other functional capacities of activated (by visible range irradiation) sugarcane mill mud over commercial composts and existing bio-fertilizers need to be evaluated for commercially viable development of specialized finished products including bio-stimulant and bio-fertilizer.

CONCLUSIONS

1. Industrial sources of carbon underwent light and dark reaction time courses similar to naturally occurring organic carbon. To our knowledge, this is the first evidence for similar photolysis reaction pathways, as opposed to dark incubation, between waste biomass and soil organic carbon. The optical methods considered in this work are applicable to trace the aging kinetics for a wide range of waste biomass intended for land application. Simple optical parameters could be used as a rapid and inexpensive means of tracing the environmental fate of byproducts. The optical methods could also be used to monitor the long-term efficacy of applied carbon of industrial sources.
2. Visible wavelength ranges induced the formation of aromatic chromophores by photolysis. Activation within the visible range could serve as a less energy intensive, safer (*vs*. UV range), and lower cost activation method to add values to biomass streams for improving the efficiency of agricultural production. Potential end products include bio-stimulants through enhanced aromaticity of the renewable soil amendment.

ACKNOWLEDGMENTS

This research was supported by the U.S. Department of Agriculture, Agricultural Research Service. Mention of trade names or commercial products is solely for the purpose of providing specific information and does not imply recommendation or endorsement by USDA. USDA is an equal opportunity provider and employer.

REFERENCES CITED

Buckley, S., McKay, G., Leresche, F., and Rosario-Ortiz, F. (2024). "Inferring the molecular basis for dissolved organic matter photochemical and optical properties," *Environ. Sci. Technol.* 58(21), 9040-9050. https://doi.org/10.1021/acs.est.3c10881

Del Vecchio, R., and Blough, N. V. (2004). "On the origin of the optical properties of humic substances," *Environ. Sci. Technol.* 38(14), 3885-3891. https://doi.org/10.1021/es049912h

Gilbert, R. A., Morris, D. R., Rainbolt, C. R., McCray, J. M., Perdomo, R. E., Eiland, B., Powell, G., and Montes, G. (2008). "Sugarcane response to mill mud, fertilizer, and soybean nutrient sources on a sandy soil," *Agron. J.* 100(3), 845-854. https://doi.org/10.2134/agronj2007.0247

Helms, J. R., Stubbins, A., Ritchie, J. D., Minor, E. C., Kieber, D. J., and Mopper, K. (2008). "Absorption spectral slopes and slope ratios as indicators of molecular weight, source, and photobleaching of chromophoric dissolved organic matter," *Limnol. Oceanogr.* 53(3), 955-969. https://doi.org/10.4319/lo.2008.53.3.0955

Lichtman, J. W., and Conchello, J. A. (2005). "Fluorescence microscopy," *Nat. Methods* 2(12), 910-919. https://doi.org/10.1038/nmeth817

Pignatello, J. J., Uchimiya, M., and Abiven, S. (2024). "Aging of biochar in soils and its implications," in: *Biochar for Environmental Management: Science, Technology, and Implementation*, J. Lehmann, S. Joseph (eds.), Taylor & Frances, London, UK, pp. 249-276.

Sharpless, C. M., Aeschbacher, M., Page, S.E., Wenk, J., Sander, M., and McNeill, K. (2014). "Photooxidation-induced changes in optical, electrochemical, and photochemical properties of humic substances," *Environ. Sci. Technol.* 48(5), 2688-2696. https://doi.org/10.1021/es403925g

Uchimiya, M., Hay, A. G., and LeBlanc, J. (2022). "Chemical and microbial characterization of sugarcane mill mud for soil applications," *Plos One* 17(8), article e0272013. https://doi.org/10.1371/journal.pone.0272013

Uchimiya, M., DeRito, C. M., and Hay, A. G. (2023). "Sugarcane mill mud-induced putative host (soybean (Glycine max))-rhizobia symbiosis in sandy loam soil," *Plos One* 18(11), article e0293317. https://doi.org/10.1371/journal.pone.0293317

Uchimiya, M., DeRito, C. M., Sevigny, J. L., and Hay, A. G. (2024). "Meta-analysis of ecological and phylogenetic biomass maturity metrics," *Waste Management* 190, 548-556. DOI: https://doi.org/10.1016/j.wasman.2024.10.023

Uchimiya, M., and Knoll, J. E. (2019). "Accumulation of carboxylate and aromatic fluorophores by a pest-resistant sweet sorghum [*Sorghum bicolor* (L.) Moench] genotype," *ACS Omega* 4(24), 20519-20529. https://doi.org/10.1021/acsomega.9b02267

Uchimiya, M., Ohno, T., and He, Z. (2013). "Pyrolysis temperature-dependent release of dissolved organic carbon from plant, manure, and biorefinery wastes," *J. Anal. Appl. Pyrol.* 104, 84-94. https://doi.org/10.1016/j.jaap.2013.09.003

Wu, B., Liu, T., Wang, Y., Zhao, G., Chen, B., and Chu, C. (2021). "High sample throughput led reactor for facile characterization of the quantum yield spectrum of photochemically produced reactive intermediates," *Environ. Sci. Technol.* 55(23), 16204-16214. https://doi.org/10.1021/acs.est.1c04608

Yan, M., Mo, S., Liu, Z., and Korshin, G. (2025). "Absorptivity inversely proportional to spectral slope in CDOM," *Environ. Sci. Technol.* 59(14), 7156-7164. https://doi.org/10.1021/acs.est.5c01019

Zherebker, A., B. Yakimov, A. Rubekina, O. Kharybin, E. I. Fedoros, I. V. Perminova, E. Shirshin and E. N. Nikolaev (2020). "Photoreactivity of humic-like polyphenol material under irradiation with different wavelengths explored by FTICR MS and deuteromethylation," *European Journal of Mass Spectrometry* 26(4), 292-300. https://journals.sagepub.com/doi/abs/10.1177/1469066720917067

Article submitted: February 23, 2026; Peer review completed: March 29, 2026; Revised version received: April 1, 2026; Accepted: April 9, 2026; Published: April 22, 2026.
DOI: 10.15376/biores.21.2.5057-5070

APPENDIX

Elemental Composition of Two Fresh Mill Mud Samples Investigated in this Study

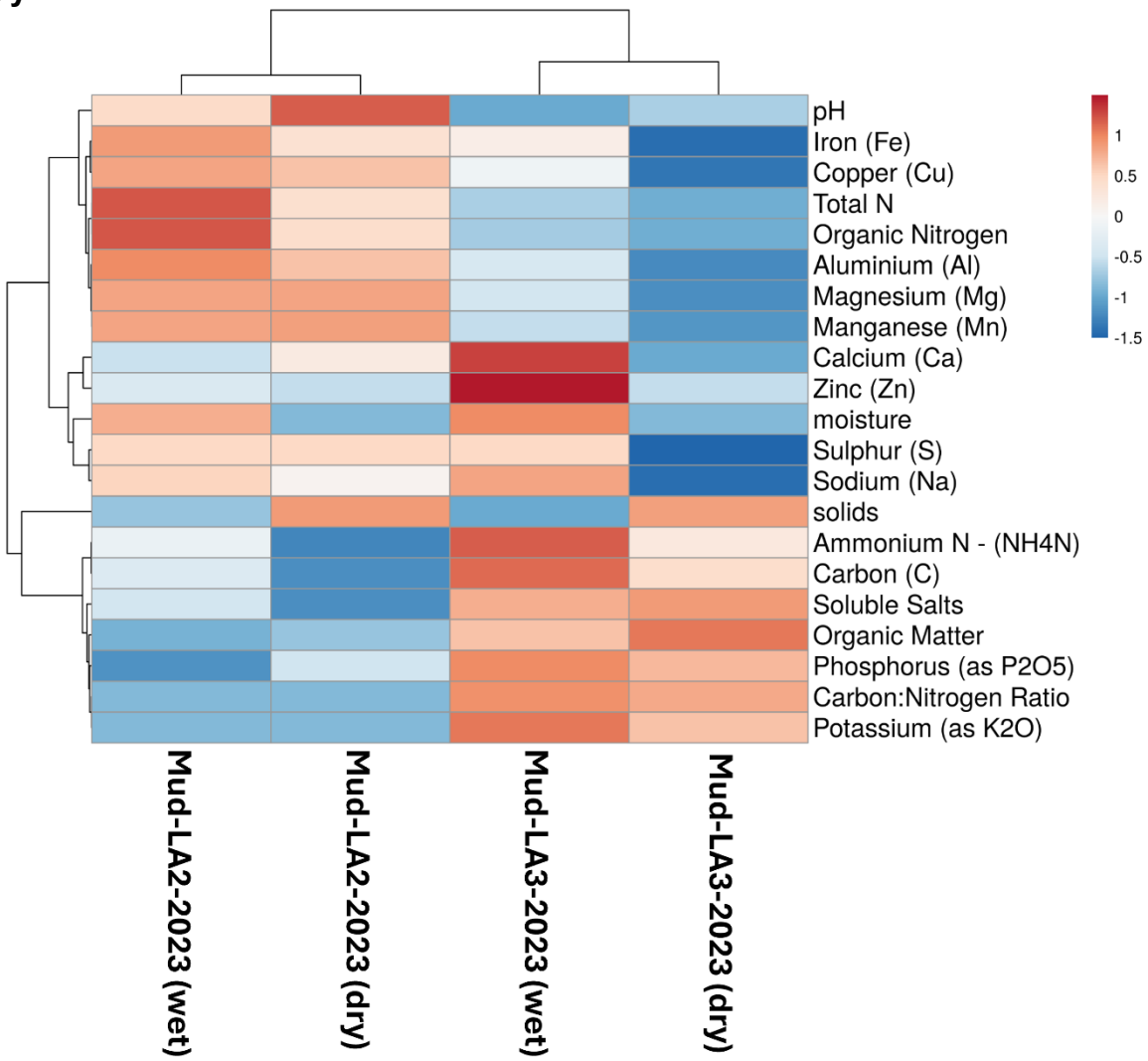

Fig. A1. Cluster analysis results for the chemical properties pertinent to fertilizer value. Columns show mill mud samples sourced from two separate factories, each in wet and dry weight basis. Rows show chemical parameters considered. Darker red indicates higher concentration, and darker blue indicates lower concentration of each chemical parameter. Mud-LA3-2023 show a red cluster represented by high organic matter, C/N, and PKN.